Diagnostic Accuracy of Noncontrast Self-navigated Free-breathing MR Angiography versus CT Angiography: A Prospective Study in Pediatric Patients with Suspected Anomalous Coronary Arteries

Moritz H. Albrecht, MD, Akos Varga-Szemes, MD, PhD, U. Joseph Schoepf, MD, John W. Nance, MD, Carlo N. De Cecco, MD, PhD, Domenico De Santis, MD, Christian Tesche, MD, Marwen H. Eid, MD, Megha Penmetsa, BS, Virginia W. Lesslie, BS, Davide Piccini, PhD, Markus Goeller, MD, Julian L. Wichmann, MD, Thomas J. Vogl, MD, Shahryar M. Chowdhury, MD, Arni Nutting, MD, Anthony M. Hlavacek, MD

Abbreviations

CTA Computed tomography angiography

MRA Magnetic resonance angiography

SN3D Free-breathing self-navigated 3D MRA

HIPAA Health Insurance Portability and Accountability Act

ECG Electrocardiography

FOV Field of view

Rationale and Objectives: To evaluate the diagnostic accuracy of a prototype noncontrast, free-breathing, self-navigated 3D (SN3D) MR angiography (MRA) technique for the assessment of coronary artery anatomy in children with known or suspected coronary anomalies, using CT angiography (CTA) as the reference standard.

Materials and Methods: Twenty-one children (15 male, 12.3 ± 2.6 years) were prospectively enrolled between July 2014 and August 2016 in this IRB-approved, HIPAA-compliant study. Patients underwent same-day unenhanced SN3D-MRA and contrast-enhanced CTA. Two observers rated the visualization of coronary artery segments and diagnostic confidence on a 3-point scale and assessed coronary arteries for anomalous origin, as well as interarterial and intramural course. Sensitivity, specificity, positive (PPV) and negative predictive values (NPV) of SN3D-MRA for the detection of coronary artery abnormalities were calculated. Interobserver agreement was assessed using Intraclass Correlation Coefficients (ICC).

Results: Fourteen children showed coronary artery abnormalities on CTA. The visualization of coronary segments was rated significantly higher for CTA compared to MRA ($p < 0.015$), except for the left main coronary artery ($p = 0.301$), with good to excellent interobserver agreement (ICC = 0.62−0.94). Diagnostic confidence was higher for CTA ($p = 0.046$). Sensitivity, specificity, PPV, and NPV of MRA were 92%, 92%, 96%, and 87% for the detection of coronary artery anomalies, 85%, 85%, 74%, and 92% for high origin, 71%, 92%, 82%, and 87% for interarterial, and 41%, 96%, 87%, and 80% for intramural course.

Acad Radiol 2019; 26:1309−1317

From the Department of Radiology and Radiological Science, Division of Cardiovascular Imaging, Medical University of South Carolina, 25 Courtenay Drive, Charleston, SC 29425 (M.H.A., A.V.-S., U.J.S., J.W.N., C.N.D.C., D.D.S., C.T., M.H.E., M.P., V.W.L., S.M.C., A.N., A.M.H.); Department of Diagnostic and Interventional Radiology, Division of Experimental and Translational Imaging, University Hospital Frankfurt, Frankfurt, Germany (M.H.A., J.L.W., T.J.V.); Department of Radiological Sciences, Oncological and Pathological Sciences University of Rome "Sapienza", Latina, Italy (D.D.S.); Department of Cardiology and Intensive Care Medicine, Heart Center Munich-Bogenhausen, Munich, Germany (C.T.); Advanced Clinical Imaging Technology, Siemens Healthcare AG, Lausanne, Switzerland (D.P.); Department of Radiology, University Hospital (CHUV) and University of Lausanne (UNIL), Lausanne, Switzerland (D.P.); Biomedical Imaging Research Institute, Cedars-Sinai Medical Center, Los Angeles, California (M.G.); Division of Pediatric Cardiology, Department of Pediatrics, Medical University of South Carolina, Charleston South Carolina (S.M.C., A.N., A.M.H.). Received October 19, 2018; revised December 9, 2018; accepted December 10, 2018. Disclosures: This study was supported in part by a research grant provided by SiemensHealthineers. Moritz H. Albrecht received speaker fees from Siemens MR Peds - 8A387 and Bracco. Carlo N. De Cecco and Akos Varga-Szemes are consultants for and/or receive research support from Guerbet and Siemens. Davide Piccini is an employee of Siemens. Julian L. Wichmann received speaker fees from Siemens and GE. Anthony M. Hlavacek receives research support from Siemens. **Address correspondence to:** U.J.S. e-mail: schoepf@musc.edu

Published by Elsevier Inc. on behalf of The Association of University Radiologists.
https://doi.org/10.1016/j.acra.2018.12.010

TR
Time of repetition

TE
Time of echo

HU
Hounsfield units

DLP
Dose-length-product

MPRs
Multi-planar reformat

MIP
Minimum-intensity projection

CA
Coronary artery

RCA
Right CA

LM
Left main CA

LAD
Left anterior descending CA

LCX
Left circumflex CA

D1
First diagonal CA

PDA
Posterior descending CA

ICC
Intraclass correlation coefficients

PPV
Positive predictive value

NPV
Negative predictive value

BMI
Body-mass-index

ALARA
"As Low As Reasonably Achievable"- principle

Conclusions: Noncontrast SN3D-MRA is highly accurate for the detection of coronary artery anomalies in pediatric patients while diagnostic confidence and coronary artery visualization remain superior with CTA.

Key Words: Magnetic Resonance Angiography; Computed Tomography Angiography; Pediatric Cardiac Imaging; Coronary Angiography; Free-breathing Self-navigated MRA; Noncontrast MRA.

Published by Elsevier Inc. on behalf of The Association of University Radiologists.

INTRODUCTION

Cross-sectional imaging modalities, such as coronary computed tomography angiography (CTA) and magnetic resonance angiography (MRA) are increasingly used in children (1–3). To date, CTA is considered the noninvasive reference standard for imaging of the coronary arteries, both in adults (4) and children (5), enabling higher spatial resolution and faster image acquisition compared to MRA. However, there remain concerns over the cumulative radiation exposure associated with CTA (6,7), especially in pediatric patients with congenital heart disease who require serial imaging follow-up (8,9) either with repeat CTA, invasive catheterization, or other image-guided procedures. Therefore, any available radiation reduction strategies should be implemented in this population. Furthermore, there are rare but notable risks associated with the intravenous administration of contrast material both for CT (10,11) and MR (12,13) examinations. Accordingly, noncontrast imaging tests without ionizing radiation are appealing for pediatric patients, particularly those who are subject to repeat imaging (14,15).

Coronary MRA is not associated with ionizing radiation; however, prior MRA approaches have been limited by user-dependent navigator placement and unpredictable imaging times due to irregular breathing patterns (16,17). Recently, a free-breathing self-navigated 3D (SN3D) radial whole heart MRA technique was introduced, which has greater scan efficiency and a reduced image acquisition time compared to traditional respiratory-navigated MRA approaches (16,18). A prior study suggests that this SN3D-MRA approach with contrast material administration provides good image quality in children with congenital heart disease (19); however, there is a lack of data regarding the diagnostic accuracy of this

technique for the detection of congenital coronary artery anomalies. Moreover, evidence is scarce regarding the robustness of SN3D-MRA when employed without contrast media administration. We hypothesized that the diagnostic accuracy of noncontrast SN3D-MRA is similar to CTA for the detection of coronary artery anomalies. Furthermore, we aimed to quantify the diagnostic performance of SN3D-MRA in the characterization of more subtle anatomical detail such as interarterial and intramural coronary artery course.

Thus, the purpose of this study was to evaluate the diagnostic accuracy of a prototype noncontrast, free-breathing coronary SN3D-MRA technique for the assessment of coronary artery anatomy in children with known or suspected coronary anomalies, using CTA as the reference standard.

MATERIALS AND METHODS

Patients

Our local Institutional Review Board approved this prospective, HIPAA-compliant study and written informed consent was obtained from each participant's guardian. From July 2014 to August 2016, 21 pediatric patients were included (15 male, mean age: 12.3 ± 2.6 years, range: 8−7 years) who required additional coronary artery imaging because of inconclusive echocardiography, and each underwent a CTA and MRA on the same day. Notably, in the routine clinical practice of our institution, patients always have to go echocardiography first before a potential CTA is performed subsequently. The group included 15 patients with known or suspected congenital coronary anomalies and 6 individuals with repaired transposition of the great arteries who had reimplantation of their coronary origins as part of their surgical repair. Subjects with an implanted cardiac device and/or arrhythmias were not included. Table 1 summarizes patient characteristics.

MR Angiography

MR image acquisition was performed using a 1.5 T system (Magnetom Avanto, Siemens Healthineers, Erlangen, Germany). No contrast media was administered and examinations were performed without anesthesia or sedation. Patients were scanned head-first in the supine position and scans were electrocardiographically (ECG)-gated. A 24-element multichannel phased-array receiver coil was integrated in the patient table and a six-element coil was placed on the anterior side of the patient for signal reception. Following the scout images, a four-chamber steady-state free-precession cine image set was acquired in a free-breathing fashion, with four averages to compensate for respiratory motion. The following typical pulse sequence parameters: field of view (FOV) = 220−340 mm^2, repetition time/echo time (TR/TE) = 2.7/1.1 ms, number of segments = 13, reconstructed phases = 25, temporal resolution = 35 ms, flip angle = 56°, number of signal averages = 3, matrix = 192 × 100, and bandwidth = 930 Hz/pixel. Parallel imaging with an acceleration factor of two was employed (Grappa, Siemens). The cine image set was retrospectively analyzed to determine the best mid-diastolic resting phase during the cardiac cycle for ECG-based synchronization of the MRA scan (20,21). Next, a coronal slab was defined, including the heart and the great vessels, to perform the prototype SN3D-MRA acquisition using the following settings: TR/TE = 3.1/1.5 ms, FOV = $(220\ mm)^3$, isotropic voxel size = 1.15 mm^3, flip angle = 115°, receiver bandwidth = 898 Hz/pixel, matrix = 192^3, and radial k-space readout with a total of 12064 radial views acquired over 377 heartbeats. Additional technical details of the SN3D-MRA technique have been described previously (16,22,23). Notably, this free-breathing and respiratory motion-corrected approach allows for 100% scan efficiency; it does not require user-dependent diaphragm navigator placement or breathing commands and enables the prediction of scan duration prior to the acquisition (16), unlike former 3D MRA techniques (2). Imaging time required for the SN3D-MRA acquisition was recorded.

CT Angiography

CTA images were acquired using a second-generation dual-source CT system (Somatom Flash, Siemens Healthcare, Forchheim, Germany) with a low tube voltage of 70−100

TABLE 1. Patient Characteristics and Findings. Diagnostic Accuracy of Noncontrast SN3D-MRA was Analyzed for the Criteria Enumerated in *Italics* Using Contrast-Enhanced CTA as the Reference Standard. S/P Refers to Status-Post Surgical Repair of Transposition of the Great Arteries. Note that Some Patients Had More than One Anomaly. [CA – Coronary Artery, RCA – Right CA, LM – Left Main CA, LAD – Left Anterior Descending, LCX – Left Circumflex, LCA Left Coronary Artery]

CA Anomaly*	RCA	*n* = 10 (3 S/P)
	LM	*n* = 8 (3 S/P)
	LAD	*n* = 3 (2 S/P)
	LCX	*n* = 6 (5 S/P)
	RCA and LM	*n* = 6 (2 S/P)
	RCA and LAD	*n* = 1 (2 S/P)
	RCA and LCX	*n* = 3 (2 S/P)
High CA Origin	RCA	*n* = 6 (2 S/P)
	LCA	*n* = 4 (2 S/P)
	RCA and LCA	*n* = 3 (2 S/P)
Interarterial Course	RCA	*n* = 5 (2 S/P)
	LCA	*n* = 2 (2 S/P)
Intramural Course	RCA	*n* = 5 (2 S/P)
	LCA	*n* = 1 (2 S/P)
RCA	originates from left coronary sinus	*n* = 4 (2 S/P)
	originates from noncoronary sinus	*n* = 1 (2 S/P)
LCA	originates from right coronary sinus	*n* = 4 (2 S/P)
	originates from RCA	*n* = 4 (2 S/P)
	independent origin of LAD and LCX	*n* = 1 (2 S/P)

kilovolt peak (kVp). Image acquisition was performed using the sequential (axial) mode with prospective ECG triggering at 70% of the R-R interval if the heart rate was <70 bpm or 40% if the heart rate was >70 bpm. Automated tube current modulation (CareDose, Siemens) was utilized, with a reference tube current time product of 256 mAs per rotation, gantry rotation time = 280 ms, and collimation = 64 × 2 × 0.6 mm.

Iodinated contrast material (Iohexol; 350 mg of organic iodine/mL, Omnipaque 350, GE Healthcare, Little Chalfont, Buckinghamshire, UK) was administered at a flow rate of 4 mL/s via an 18-gauge intravenous cannula in a vein of the antecubital fossa. The standard contrast media dose of 60 mL could be adjusted according to patient's body weight to a maximum of 80 mL and was followed by a 40 mL saline chaser bolus. Image acquisition was automatically initiated 2 seconds after a threshold of 100 Hounsfield units (HU) was reached in a region of interest placed in the descending aorta.

CT raw data were reconstructed using a standard medium-sharp (I26f) reconstruction algorithm and sonogram affirmed iterative reconstruction (Safire, strength level 3, Siemens). Images were reconstructed with 0.75 mm slice thickness at 0.3 mm increments. The effective dose of each CTA examination was calculated by multiplying the dose-length-product (DLP) with conversion factors based on gender and age, as previously described (24).

Image Analysis

SN3D-MRA and CTA datasets were independently reviewed by two observers with 7 and 4 years of experience in cardiac imaging, respectively. Readers were blinded to clinical information and in particular, potential prior procedures. Interpretations were performed on 3D multi-modality workstations (TeraRecon, Aquarius iNtuition Viewer, version 4.4.12, TeraRecon Inc., Foster City, CA). The examinations were assessed in randomized order and CTA and MRA images were evaluated separately. Readers started with the MRA analysis and observed a minimum one-week time interval between analyses of CTA examinations in order to minimize potential recall bias. Transverse, coronal, and sagittal multi-planar reformats (MPRs) were evaluated and image orientation could be freely adjusted. Preset window settings could be modified to optimize image contrast according to reader preference. In addition, reviewers were permitted to switch from MPR to maximum-intensity projection (MIP) series as necessary. Readers were blinded to clinical indication, patient age and gender.

First, the quality of coronary artery visualization was rated both for SN3D-MRA and CTA for the right (RCA), left main (LM), left anterior descending (LAD), left circumflex (LCX), first diagonal (D1), and posterior descending (PDA) coronary arteries using the following 3-point scale: 1 = insufficient visualization, 2 = adequate visualization, and 3 = excellent visualization. Diagnostic confidence was scored overall, as well as for the assessment of coronary artery anomalies: 1 = insufficient diagnostic confidence, 2 = adequate diagnostic confidence, and 3 = excellent diagnostic confidence.

Second, the two readers rated the presence of coronary artery anomalies using SN3D-MRA images for the RCA, LM, LAD, and LCX dichotomously as present or absent. Any abnormality in the location of the coronary artery origin was considered anomalous, resulting from either a congenital coronary abnormality or a postsurgical condition (e.g., coronary reimplantation during repair of transposition of the great arteries), recognizing that some patients may have both congenital and postsurgical anomalies. A high coronary origin, also known as origin from the ascending aorta distal to the aortic sinuses as well as the criteria of interarterial and intramural coronary artery course were included as anomalies. However, clinically insignificant abnormalities such as an eccentric origin from the appropriate sinus were not included as an anomaly for the purposes of this study. Furthermore, the following descriptors of coronary artery course were rated dichotomously as present or absent for the RCA, LM, LAD, and LCX: high origin, interarterial course, and intramural course within the aortic wall.

The radiological CTA reports from clinical routine served as the reference standard for the particular analysis of SN3D-MRA diagnostic accuracy. The original CTA reports were reconfirmed by an investigator with 10 years of experience in cardiac imaging, who reviewed the CTA examinations and did not participate in the actual rating sessions.

Statistical Evaluation

Dedicated software was used for statistical analysis (MedCalc Statistical Software Version 12.7.2, MedCalc Software bvba, Ostend, Belgium). Data were expressed as medians and arithmetic means. The Kolmogorov-Smirnov test was used to assess the normality of data distribution. Normally distributed data were assessed using a Student *t* test. Data showing no Gaussian distribution were analyzed with the Wilcoxon matched-pairs test. Interobserver agreement for the ratings was assessed by means of Intraclass Correlation Coefficients (ICC) and interpreted as follows: <0.2 = poor, 0.2−0.4 = acceptable, 0.41−0.6 = moderate, 0.61−0.8 = good, and >0.8 = excellent agreement.

Sensitivity, specificity, positive predictive value (PPV), and negative predictive value (NPV) were calculated on both a per-patient and per-vessel basis for the respective coronary artery segments.

Results below the $\alpha = 0.05$ threshold were considered statistically significant and 2-sided p-values (*P*) were reported.

RESULTS

No complications occurred during the CTA or SN3D-MRA examinations. Patients mean BMI was 21.3 ± 6.1 kg/m^2, range: 12−32 kg/m^2. CTA images were acquired with a tube voltage of 79.0 ± 8.3 kVp (70 kVp in 6, 80 kVp in 13, and 100 kVp in 2 patients. These tube potential settings resulted in a mean DLP of 57.5 ± 40.8 and an average age /

gender adjusted effective radiation dose equivalent of 0.9 ± 0.5 mSv (24). On average, 62 ± 16 mL of contrast media was administered for CTA image acquisitions. The time required for the SN3D-MRA acquisition was 5.3 ± 1.7 minutes on average.

Coronary Arteries

Evaluation of CTA images revealed coronary artery abnormalities in 14 of 21 children (66.6%), which are characterized in detail in Table 1. Representative examples of CA anomalies visualized by means of CTA and SN3D-cMRA are shown in Fig. 1 and 2.

Visualization of Coronary Arteries

Scores for visualization of all coronary artery segments were significantly higher ($p < 0.015$) for CTA compared to SN3D-MRA images, with the exception of the LM coronary artery ($p = 0.301$). Among CTA and MRA imaging modalities, scores differed more distinctly (all with $p < 0.001$) for the visualization of distal coronary artery segments (PDA and D1; mean scores, CTA = 2.6 and MRA = 1.7), than proximal coronary arteries (RCA, LM, LAD, and LCX; mean scores, CTA = 2.8 and MRA = 2.4). Cumulative interobserver agreement was good for CTA (ICC = 0.79) and excellent for MRA (ICC = 0.90) evaluation. Scores for visualization of coronary artery segments and interobserver agreement are summarized in Table 2 and presented in Fig 3.

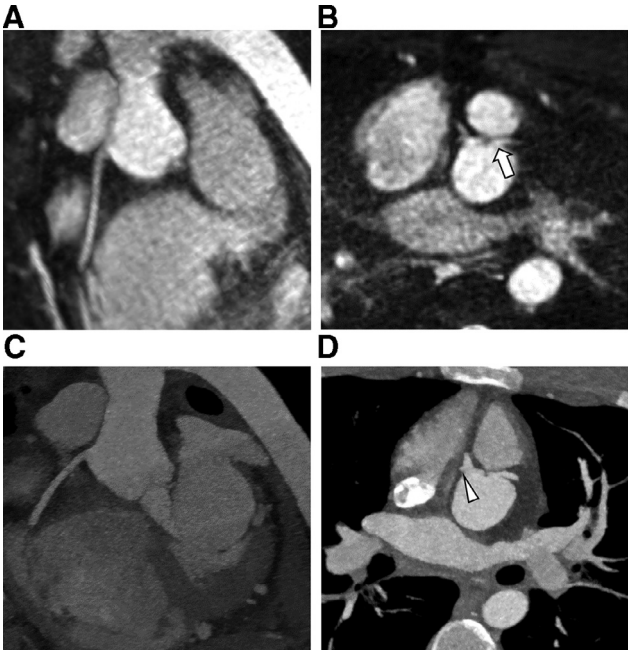

Figure 1. Noncontrast self-navigated 3D coronary magnetic resonance angiography (SN3D-MRA, A and B) with corresponding coronary computed tomographic angiography (CTA) (C and D) acquired in a 14-year-old boy status-post surgical correction of transposition of the great arteries. Both imaging tests reveal a high origin of the re-implanted right (RCA) and left main coronary artery (LM). Both MRA and CTA visualize the atypical origin of the left circumflex coronary (LCX) from the RCA (*arrowhead*). Furthermore, the LM is slightly compressed between ascending aorta and main pulmonary artery (*arrow*). Thus, the relevant diagnostic information regarding proximal CA anatomy is provided by MRA without ionizing radiation or the need for contrast-media administration. However, image quality was rated higher for CTA.

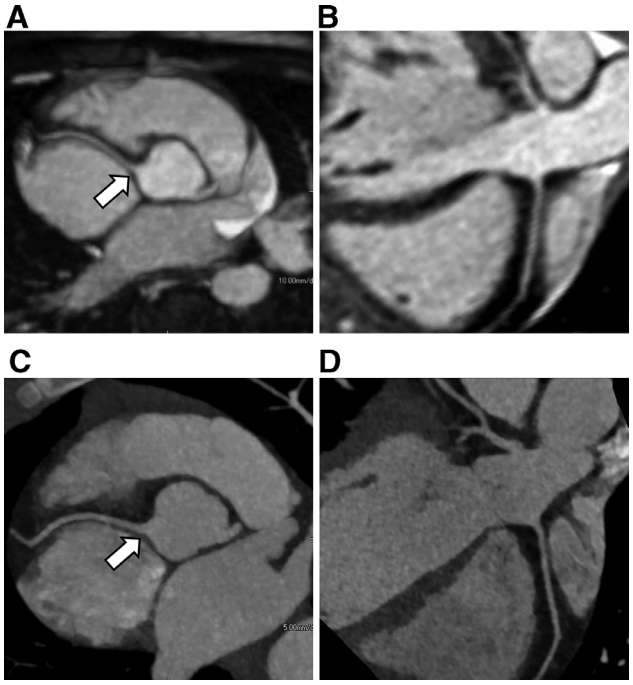

Figure 2. This 10-year-old girl had multiple recent episodes of chest pain. Echocardiography was inconclusive regarding a possible coronary anomaly. Both SN3D -MRA (A, B) and CTA (C, D) showed an anomalous origin of the RCA (*arrows*) from the "noncoronary" sinus.

Diagnostic Confidence

Reader confidence regarding all criteria (assessment of coronary artery anomalies, high origin, interarterial course, and intramural course) was significantly higher ($p < 0.046$) for CTA compared to MRA images. The difference between CTA and MRA scores was greatest for intramural course (difference between the median score = 1 and mean score = 0.5, Fig 4). Overall diagnostic confidence was greater ($P = 0.007$) for the evaluation of CTA (mean score = 2.9, ICC = 0.89) in comparison to MRA datasets (mean score = 2.6, ICC = 0.89). Additional data are presented in Table 3 and Fig 5.

Diagnostic Accuracy

The overall patient-based diagnostic accuracy in coronary artery anomaly detection of SN3D-MRA images with CTA as the reference standard was 92.8% with excellent agreement (ICC = 0.94). Diagnostic accuracy was 85.7% for both high coronary artery origin and interarterial course detection with excellent (ICC = 0.89) and good agreement (ICC = 0.71),

TABLE 2. Analysis of CA Visualization. Average Qualitative Scores of Both Observers Indicate that Each Coronary Segment was Better Visualized Using CTA. Interobserver Agreement Ranged From Moderate to Excellent. *p* was <0.05 for All ICC Values

Analysis of Coronary Segment Visualization		RCA	LM	LAD	LCX	D1	PDA
Median [Range] (Mean)	CTA	3.0 [2–3] (2.83)	3.0 [2–3] (2.81)	3.0 [2–3] (2.88)	3.0 [2–3] (2.83)	3.0 [2–3] (2.64)	3.0 [1–3] (2.59)
	MRA	3.0 [2–3] (2.54)	3.0 [2–3] (2.73)	3.0 [2–3] (2.38)	2.0 [1–3] (2.09)	1.5 [1–3] (1.59)	2.0 [1–3] (1.88)
		$p = 0.015$	$p = 0.301$	$P < 0.001$	$P < 0.001$	$P < 0.001$	$P < 0.001$
ICC [95% CI]	CTA	0.91 [0.78–0.96]	0.87 [0.69–0.95]	0.87 [0.69–0.95]	0.70 [0.26–0.87]	0.78 [0.45–0.91]	0.62 [0.06–0.84]
	MRA	0.94 [0.87–0.97]	0.93 [0.84–0.97]	0.88 [0.72–0.95]	0.87 [0.68–0.94]	0.91 [0.78–0.96]	0.87 [0.69–0.95]
		$P < 0.001$	$P < 0.001$	$P < 0.001$	$P < 0.001$	$P < 0.001$	$P < 0.001$

Abbrebiations: CA, coronary artery; CI, confidence interval; CTA, coronary CT angiography; MRA, coronary MR angiography; ICC, intraclass correlation coefficient.

respectively. The lowest diagnostic accuracy was found for intramural course, at 80.9%, with moderate agreement (ICC = 0.39).

Additional data for sensitivity, specificity, PPV and NPV, particularly regarding segment-based accuracy for coronary artery anomaly detection, are provided in Table 4.

DISCUSSION

The aim of this study was to evaluate the image quality, diagnostic confidence, and diagnostic accuracy of noncontrast SN3D-MRA for the detection of coronary artery anomalies in pediatric patients, using CTA as the reference standard.

Although the quality of coronary artery visualization and diagnostic confidence was rated lower using MRA compared to CTA, we demonstrated that MRA allows for excellent diagnostic accuracy in the detection of coronary artery anomalies, with sensitivity, specificity, PPV, and NPV ranging from 87%– 96%. Furthermore, in our prospective patient cohort, MRA ruled out an interarterial course and a high origin of coronary arteries with reasonable reliability, given its specificity and NPV greater than 85%. Considering the "As Low As Reasonably Achievable" (ALARA) principle (6), which stresses the importance of minimizing radiation exposure in children, our results suggest that SN3D-MRA provides a clinically viable alternative, dose-saving approach in pediatric patients with suspected coronary artery malformations and anomalies. However, our data also indicate that MRA has limited value in subtle characterization of coronary artery anomalies, such as intramural course, due to its

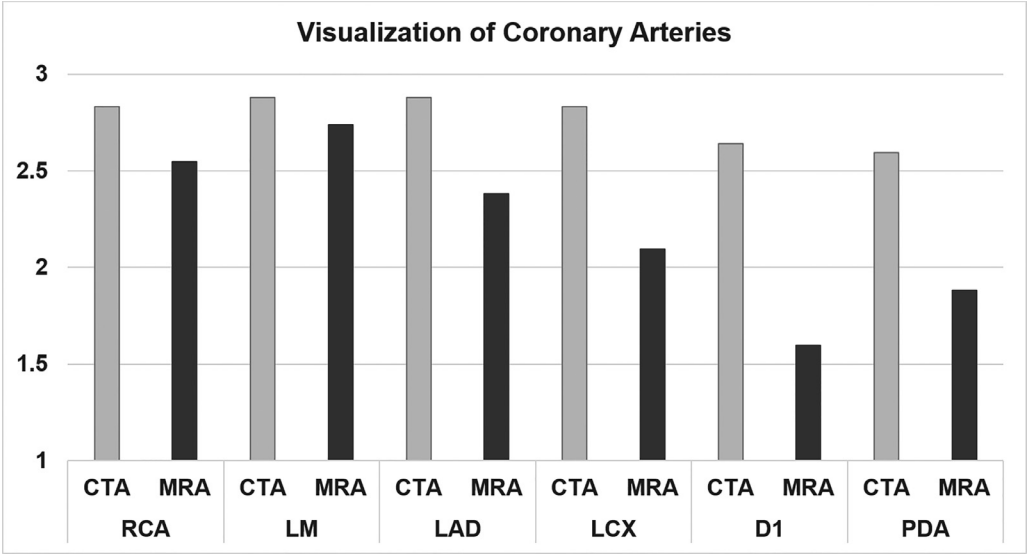

Figure 3. While the ratings for LM coronary artery visualization were comparable ($p = 0.301$), visualization of the other segments was scored significantly higher for CTA ($p < 0.015$). Notably, the difference between CTA and MRA scores was greater for distal CA segments (PDA and D1) than proximal coronary artery segments. [CTA – CT angiography, MRA – MR angiography, CA – coronary artery, LM – left main, LAD – left anterior descending, LCX – left circumflex, D1 – first diagonal branch, PDA – posterior descending artery].

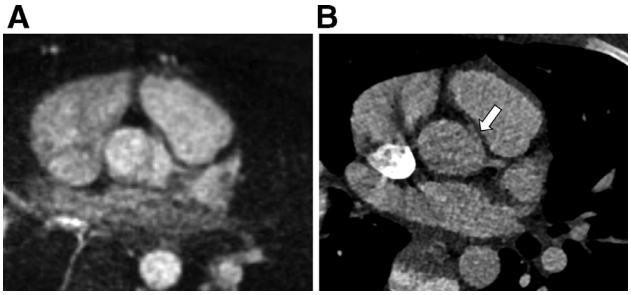

Figure 4. This 11-year-old boy showed an anomalous origin of the RCA from the left sinus of Valsalva with a short, proximal intramural segment using MRA (A) and CTA (B) images. The intramural segment is best visualized in CTA images (*arrow*). Furthermore, the RCA has an interarterial course between the aorta/right ventricular outflow tract and the main pulmonary artery, which is evident in both MRA and CTA images.

insufficient sensitivity. In this context, our results may also suggest that a potential concomitant slit-like coronary ostium may not be appropriately visualized on SN3D-MRA.

Several previous studies have shown the technical feasibility of the free-breathing SN3D-MRA approach (16,18) although a direct comparison with coronary CTA had not been performed to date. These prior experiences demonstrated higher success rates, artifact reduction, and shorter imaging times in comparison to previous MRA techniques which utilize user-dependent navigator placement (25). In addition, our results show that SN3D-MRA exams allow for acceptable visualization of the RCA, LM, LAD, and LCX, compared to CTA. In more distal branches, scores for the visualization of coronary artery segments were substantially lower for SN3D-MRA in comparison to CTA. This observation is in accordance with the findings of other investigators, who suggested that MRA should be preferably chosen for the evaluation of proximal coronary artery segments (26). Therefore, our results suggest that CTA should be preferred over SN3D-MRA in cases of suspected pathology in the distal coronary arteries or intramural coronary course.

Notably, observer diagnostic confidence for MRA was lower than CTA both for the evaluation of different coronary arteries and overall. However, since diagnostic accuracy was not negatively affected, our data supports SN3D-MRA as a substitute for, or gate-keeper examination to CTA, as well as a potential screening test in a priori healthy subjects with suspected coronary artery anomalies.

In accordance with the high diagnostic accuracy reported in our study, Tangcharoen et al found high sensitivity and specificity for coronary artery anomaly detection using contrast-enhanced free-breathing MRA in a study including 58 pediatric patients with 4 subjects positive for coronary artery anomalies (27). Post et al also found sensitivity and specificity of 100% using contrast MRA in a cohort of 38 patients that included 19 patients with an anomalous coronary course (26). Our data goes further, suggesting that a high sensitivity and specificity of 92.8% for the detection of anomalous coronary artery course can be achieved without the use of contrast media using the SN3D-MRA technique. Notably, another investigation has also demonstrated the usefulness of noncontrast MRA for the evaluation of coronary artery anomalies and variants in adults; however, the study lacked a reliable reference standard such as CTA and definitive diagnostic accuracy parameters (28).

Furthermore, several studies with smaller patient cohorts focused on the accuracy of contrast-enhanced CTA for coronary artery anomaly detection and found sensitivity values of up to 100% (29,30). Our result for the detection of coronary artery anomalies suggests that the diagnostic accuracy of MRA closely approaches that of CTA, the current noninvasive reference standard imaging test for coronary artery imaging (31).

A recent study by He et al investigated the diagnostic performance of the SN3D-MRA technique, using invasive catheterization as a reference standard in adults and showed high diagnostic accuracy, even for coronary artery stenosis detection (15). Although our study population was pediatric, we believe our results should prompt further investigation into the feasibility of using the SN3D-MRA technique for coronary artery characterization in adults.

Both iodinated (32,33) and gadolinium-based contrast media (13) are associated with rare but potentially harmful

TABLE 3. Diagnostic Confidence. Mean Qualitative Ratings for Diagnostic Confidence were Higher for CTA vs MRA Evaluation. Interobserver Agreement Ranged From Moderate to Excellent. *p* was <0.05 for All ICC Values

Diagnostic Confidence		CA Anomaly	High Origin	Interarterial Course	Intramural Course	Overall
Median [Range] *(Mean)*	CTA	3.0	3.0	3.0	3.0	3.0
		[3]	[2–3]	[2–3]	[2–3]	[2–3]
		(2.97)	(2.95)	(2.95)	(2.88)	(2.97)
	MRA	3.0	3.0	3.0	2.0	3.0
		[2–3]	[2–3]	[2–3]	[1–3]	[2–3]
		(2.61)	(2.73)	(2.73)	(2.35)	(2.66)
		$p = 0.006$	$p = 0.046$	$p = 0.039$	$p = 0.001$	$p = 0.007$
ICC [95% CI]	CTA	0.89	0.81	0.94	0.87	0.89
		[0.73–0.95]	[0.54–0.92]	[0.87–0.97]	[0.69–0.95]	[0.73–0.95]
	MRA	0.80	0.80	0.87	0.73	0.89
		[0.51–0.92]	[0.52–0.92]	[0.70–0.95]	[0.34–0.89]	[0.73–0.95]
		$p < 0.001$	$p < 0.001$	$p < 0.001$	$p < 0.001$	$p < 0.001$

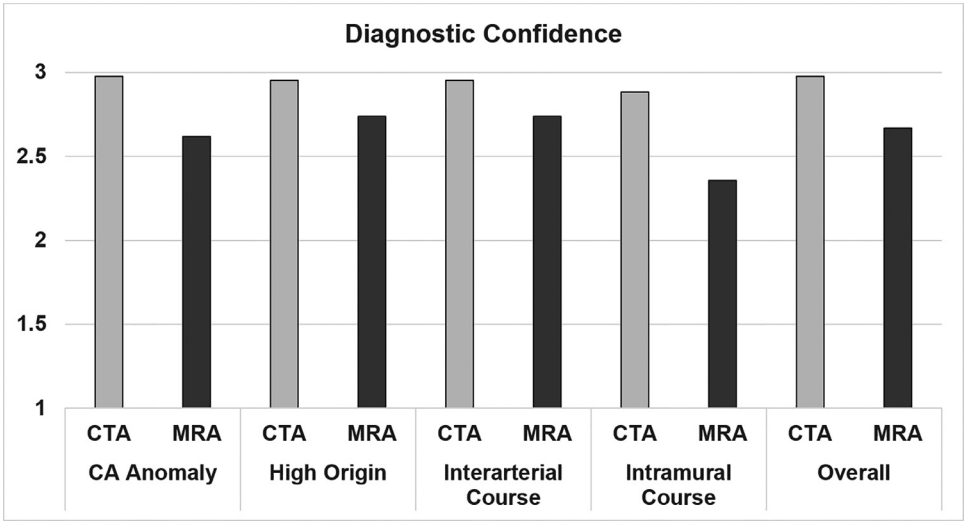

Figure 5. The difference in diagnostic confidence between CTA and MRA was greatest for the assessment of intramural course of coronary arteries. [CA – coronary arteries].

adverse events. More recently, concerns have also been raised about cerebral gadolinium retention, especially after serial MR imaging procedures in pediatric patients (12). Our proposed approach has the potential to mitigate contrast-related risks in these patients, as our data demonstrates the feasibility and accuracy of the SN3D-MRA technique while avoiding contrast agents entirely.

The following limitations must be considered when interpreting our results. Firstly, our patient cohort was small. Although acquiring comparative, successive CTA and MRA data in children is challenging, future large-scale studies would be beneficial to confirm or extend our results. In addition, although same-day CTA and MRA data were acquired for each patient and compared regarding observer confidence and coronary artery visualization, the ultimate diagnostic accuracy of CTA could not be assessed since no additional independent reference standard was available. Furthermore, our results may only apply to pediatric patients older than 8 years and additional sedation or anesthesia may be required when acquiring SN3D-MRA images in younger individuals. It is also important to mention that a remaining recall bias regarding the MRA and CTA evaluations cannot be completely excluded. Moreover, a dedicated analysis of diagnostic accuracy for the detection of coronary slit-like ostium could not be performed, due to a low prevalence in our relatively small patient cohort. Another potential limitation of our study is the fact that patients with both congenital and postsurgical coronary abnormalities were included. The authors recognize that the clinical indications and significance of coronary abnormalities differs between these two

TABLE 4. Diagnostic Accuracy of SN3D-MRA. Values Refer to CA Anomalies (Both Per-Patient And Per-Vessel) and Malignant CA Criteria (All Per-Patient). Interobserver Agreement Ranged From Acceptable to Excellent. The 95% CI of ICC Values are Given in Square Brackets. *p* was < 0.05 for All ICC Values

Diagnostic Accuracy of MRA	Sensitivity	Specificity	PPV	NPV	ICC
CA Anomaly per-patient	92.8%	92.8%	96.1%	87.5%	0.81 [0.55–0.92]
CA Anomaly RCA	90.0%	90.9%	89.8%	91.6%	0.90 [0.76–0.96]
CA Anomaly LM	93.8%	96.2%	93.8%	96.1%	0.88 [0.72–0.95]
CA Anomaly LAD	83.3%	97.2%	83.3%	97.2%	0.75 [0.40–0.90]
CA Anomaly LCX	83.3%	96.4%	90.0%	93.3%	0.77 [0.45–0.90]
High CA Origin	85.7%	85.7%	74.6%	92.8%	0.89 [0.74–0.95]
Interarterial Course	71.4%	92.9%	82.9%	87.1%	0.71 [0.28–0.88]
Intramural Course	41.7%	96.7%	87.5%	80.7%	0.39 [-0.49–0.75]

populations. However, the intent of this study was to document the diagnostic utility and accuracy of noncontrast SN3D-MRA in visualizing these anomalies whenever clinically necessary.

CONCLUSIONS

We demonstrated that non-contrast SN3D-MRA studies provide considerable diagnostic accuracy regarding the detection of anomalies, high origin, and inter-arterial course of the coronary arteries. In children with suspected coronary artery malformations, this may enable a reduction in ionizing radiation and contrast media volume. However, contrast-enhanced CTA remains the superior imaging technique currently in terms of diagnostic confidence and visualization of more distal coronary artery branches and characterization of subtle anatomical detail such as intramural coronary course.

REFERENCES

1. Dacher J-N, Barre E, Durand I, et al. CT and MR imaging in congenital cardiac malformations: Where do we come from and where are we going? Diagn Interv Imaging 2016; 97:505–512.
2. Stuber M, Weiss RG. Coronary magnetic resonance angiography. J Magn Reson Imaging JMRI 2007; 26:219–234.
3. Meinel FG, Henzler T, Schoepf UJ, et al. ECG-synchronized CT angiography in 324 consecutive pediatric patients: spectrum of indications and trends in radiation dose. Pediatr Cardiol 2015; 36:569–578.
4. Hou Y, Ma Y, Fan W, et al. Diagnostic accuracy of low-dose 256-slice multidetector coronary CT angiography using iterative reconstruction in patients with suspected coronary artery disease. Eur Radiol 2014; 24:3–11.
5. Sorensen C, Gach P, Pico H, et al. Cardiac CT or MRI in pediatric practice: Which one to choose? Diagn Interv Imaging 2016; 97:513–517.
6. Hausleiter J. Estimated radiation dose associated with cardiac CT angiography. JAMA 2009; 301:500.
7. Leschka S, Stolzmann P, Schmid FT, et al. Low kilovoltage cardiac dual-source CT: attenuation, noise, and radiation dose. Eur Radiol 2008; 18:1809–1817.
8. Bacher K, Bogaert E, Lapere R, et al. Patient-specific dose and radiation risk estimation in pediatric cardiac catheterization. Circulation 2005; 111:83–89.
9. Hoffmann A, Engelfriet P, Mulder B. Radiation exposure during follow-up of adults with congenital heart disease. Int J Cardiol 2007; 118:151–153.
10. Davenport MS, Khalatbari S, Cohan RH, et al. Contrast material-induced nephrotoxicity and intravenous low-osmolality iodinated contrast material: risk stratification by using estimated glomerular filtration rate. Radiology 2013; 268:719–728.
11. Bartorelli AL, Marenzi G. Contrast-induced nephropathy. J Intervent Cardiol. 2008; 21:74–85.
12. Roberts DR, Chatterjee AR, Yazdani M, et al. Pediatric patients demonstrate progressive T1-weighted hyperintensity in the dentate nucleus following multiple doses of gadolinium-based contrast agent. Am J Neuroradiol 2016; 37:2340–2347.
13. Shellock FG, Spinazzi A. MRI safety update 2008: Part 1, MRI contrast agents and nephrogenic systemic fibrosis. Am J Roentgenol. 2008; 191:1129–1130.
14. Ait-Ali L, Andreassi MG, Foffa I, et al. Cumulative patient effective dose and acute radiation-induced chromosomal DNA damage in children with congenital heart disease. Heart 2010; 96:269–274.
15. He Y, Pang J, Dai Q, et al. Diagnostic performance of self-navigated whole-heart contrast-enhanced coronary 3-T MR angiography. Radiology 2016; 281:401–408.
16. Piccini D, Monney P, Sierro C, et al. Respiratory Self-navigated Postcontrast Whole-Heart Coronary MR Angiography: Initial Experience in Patients. Radiology 2014; 270:278–286.
17. Kato S, Kitagawa K, Ishida N, et al. Assessment of coronary artery disease using magnetic resonance coronary angiography: A national multicenter trial. J Am Coll Cardiol 2010; 56:983–991.
18. Piccini D, Littmann A, Nielles-Vallespin S, et al. Respiratory self-navigation for whole-heart bright-blood coronary MRI: Methods for robust isolation and automatic segmentation of the blood pool. Magn Reson Med 2012; 68:571–579.
19. Monney P, Piccini D, Rutz T, et al. Single centre experience of the application of self-navigated 3D whole heart cardiovascular magnetic resonance for the assessment of cardiac anatomy in congenital heart disease. J Cardiovasc Magn Reson 2015; 9:55.
20. Lai P, Bi X, Jerecic R, Li D. A respiratory self-gating technique with 3D-translation compensation for free-breathing whole-heart coronary MRA. Magn Reson Med 2009; 62:731–738.
21. Ishida M, Sakuma H. Coronary MR angiography revealed: how to optimize image quality. Magn Reson Imaging Clin N Am 2015; 23:117–125.
22. Piccini D, Bonanno G, Ginami G, et al. Is there an optimal respiratory reference position for self-navigated whole-heart coronary MR angiography?: Optimal Respiratory Reference for Coronary MRA. J Magn Reson Imaging 2016; 43:426–433.
23. Piccini D, Feng L, Bonanno G, et al. Four-dimensional respiratory motion-resolved whole heart coronary MR angiography: Respiratory motion-resolved coronary MRA. Magn Reson Med 2016; 77:1473–1484.
24. Deak PD, Smal Y, Kalender WA. Multisection CT Protocols: Sex- and Age-specific Conversion Factors Used to Determine Effective Dose from Dose-Length Product. Radiology 2010; 257:158–166.
25. Forman C, Piccini D, Grimm R, et al. Reduction of respiratory motion artifacts for free-breathing whole-heart coronary MRA by weighted iterative reconstruction: Weighted Iterative Reconstruction for CMRA. Magn Reson Med 2015; 73:1885–1895.
26. Post JC, van Rossum AC, Bronzwaer JGF, et al. Magnetic resonance angiography of anomalous coronary arteries : A new gold standard for delineating the proximal course? Circulation 1995; 92:3163–3171.
27. Tangcharoen T, Bell A, Hegde S, et al. Detection of coronary artery anomalies in infants and young children with congenital heart disease by using MR imaging. Radiology 2011; 259:240–247.
28. Gharib AM, Ho VB, Rosing DR, et al. Coronary artery anomalies and variants: technical feasibility of assessment with coronary MR angiography at 3 T. Radiology 2008; 247:220–227.
29. Shi H, Aschoff AJ, Brambs H-J, et al. Multislice CT imaging of anomalous coronary arteries. Eur Radiol 2004; 14:2172–2181.
30. Datta J, White CS, Gilkeson RC, et al. Anomalous coronary arteries in adults: depiction at multi–detector row CT angiography. Radiology 2005; 235:812–818.
31. Raimondi F, Bonnet D. Imaging of congenital anomalies of the coronary arteries. Diagn Interv Imaging 2016; 97:561–569.
32. Davenport MS, Khalatbari S, Cohan RH, et al. Contrast material-induced nephrotoxicity and intravenous low-osmolality iodinated contrast material: risk stratification by using estimated glomerular filtration rate. Radiology 2013; 268:719–728.
33. Bucher AM, De Cecco CN, Schoepf UJ, et al. Is contrast medium osmolality a causal factor for contrast-induced nephropathy? BioMed Res Int. 2014; 2014:931413.